2

POROUS STRUCTURE

2.1 INTRODUCTION

The design of a pebble bed such as a PBR relies heavily on the mechanisms of heat and mass transfer and pressure drop of the fluid flowing through the bed of solids (Kugeler & Schulten, 1989; KTA, 1981). The mechanisms in turn are all sensitive to the porous structure of the packed bed (White & Tien, 1987:291). Most of the difficulties encountered in predicting the effective thermal conductivity have been attributed to the modelling of the microstructure in a porous matrix (Aichlmayr, 1999:9). Therefore, before any rigorous heat transfer analysis is attempted in a randomly packed bed of spheres, a thorough understanding of the structural arrangement at hand is required.

One fundamental difference between pebble beds must be highlighted i.e. a stagnant and a slowly moving pebble bed. A stagnant pebble bed consists of a packed bed with no moving pebbles, where a slowly moving pebble bed is a pebble bed where pebbles are removed at the bottom and replaced at the top. Reactors such as the Arbeitsgemeinschaft Versuchsreaktor (AVR), Thorium High-Temperature nuclear Reactor (THTR), High Temperature Reactor (HTR-10) and the PBMR have all been designed with a slowly moving pebble bed for continuous fuel loading. The core structures of these reactors have at least in part been designed with dimples/grooves at the surface of the inner and outer reflector to avoid the order-effect (Von Der Decken & Lange, 1990:156).

This chapter and study as whole will focus on various methods for analysing the porous structure in a stagnant annular packed bed, which are randomly packed. Therefore, the effects of dimples or grooves at the surface of the inner and outer reflectors are not taken into consideration, because it is consider being a detail which could be evaluated in future.

2.2 ANALYSING A RANDOMLY PACKED MONO-SIZED SPHERICAL PACKED BED

The geometry of annular randomly packed beds can be subdivided into three different regions: the inner reflector wall annulus region, the bulk-packing region and the outer reflector region. The porous structure varies sharply near any wall, as the geometry of the packing is disrupted in this region. This wall effect is composed of two separate components namely the effect of the sidewall (radial direction) and the effect of the top-bottom wall (axial direction), referred to by Zou & Yu (1995:1504) as the thickness effect. Both of these effects were investigated owing to their importance for all the associated heat transfer and fluid flow phenomena.

In this study, the wall region is subdivided into two regions, namely the wall region defined as $0 \leq z \leq 0.5$ and the near-wall region defined as $0.5 < z \leq 5$ as displayed in Figure 2.1, where z is the number of pebble diameters away from any wall.

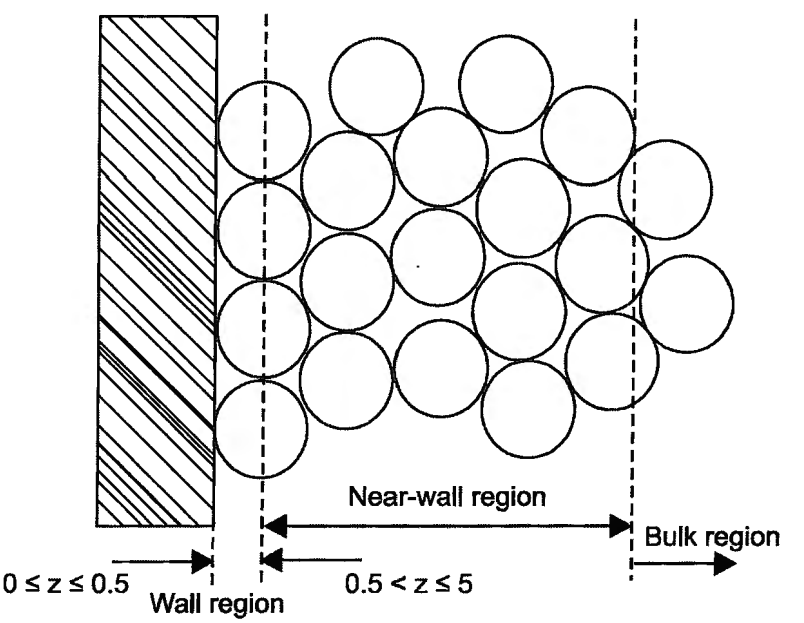

Figure 2.1: The various packing regions defined in this study

2.2.1 POROSITY

Porosity is defined as the ratio between the void volume and the total volume, also known as the void fraction (Liu *et al.*, 1999:438). It is also defined as one minus the packing density δ and is the most basic parameter for characterising the microstructure in a porous matrix.

Assuming volume-based porosity to be equivalent to area-based porosity, the following is obtained:

$$\varepsilon = 1 - \delta \tag{2.1}$$

$$\varepsilon = \frac{V_{Void}}{V_{Total}} = 1 - \frac{\sum A_{Solid}}{A_{Total}} \tag{2.2}$$

Various researchers have endeavoured to obtain the radial voidage variation of packed beds in the bulk and near-wall region experimentally (Benenati & Brosilow, 1962:359; Goodling *et al.*, 1983:23). Although the empirical research was approached in many different ways, the results are still in general agreement. A good overview of the experimental methods used by the various researchers is given in De Klerk (2003:2022). However, Mueller (1999:2458) noted that there is no published experimental data on radial void fraction distributions for annular packed beds. As annular packed beds have two walls that can simultaneously affect the void fraction distribution, it is essential to explore this further.

Du Toit (2008:3073) investigated this by constructing two sets of experiments, representing two scale models of the proposed HTTU geometry (HTTU 1-exp and HTTU 2-exp) and two scale models of the proposed annular PBMR geometry (PBMR 1-exp and PBMR 2-exp). A similar approach to that of Goodling *et al.* (1983:23) was followed to manufacture the packed beds and obtain the results. The spheres consisted of 3.6 mm lead balls and the interstices were filled with epoxy resin, with the geometrical arrangement resulting in $d_p/W = 14.12$. These geometrical packing parameters are illustrated graphically in Figure 2.2.

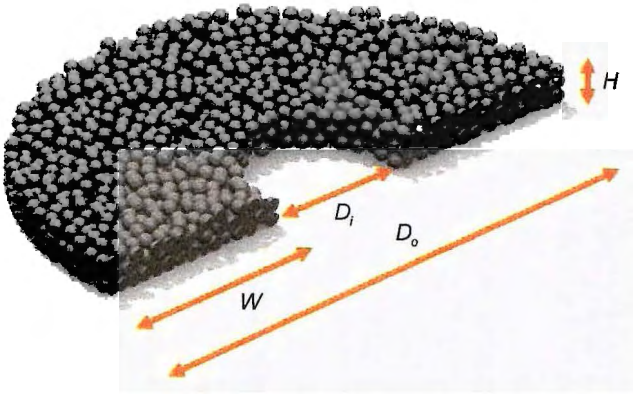

Figure 2.2: Geometrical parameters for an annular packed bed

Du Toit (2008:3073) noted that the HTTU and PBMR experimental results demonstrate the same damped oscillatory behaviour in the variation of the porosity in the radial direction between $0 \le z \le 5$, ranging from a maximum at the walls to the bulk value in the centre part of the annulus, as shown in Figure 2.3. For this reason, the wall effect both in the radial and axial direction is defined in this study as occurring at a distance of five pebble diameters $0 \le z \le 5$ away from any wall, owing to the porosity oscillations disappearing roughly at $z \ge 5$.

Packing of spheres in a container can be modelled using DEM codes, such as the so-called Particle Flow Code Three-Dimensional (PFC3D). Using such a numerically packed bed, Du Toit (2002:1) developed a method to determine the porosity variations in the axial and radial directions. Further, Du Toit (2008:3073) compared the numerically calculated radial porosity results with those obtained experimentally and good agreement was observed. The results displayed in Figure 2.3 were obtained for both the PBMR and HTTU packings.

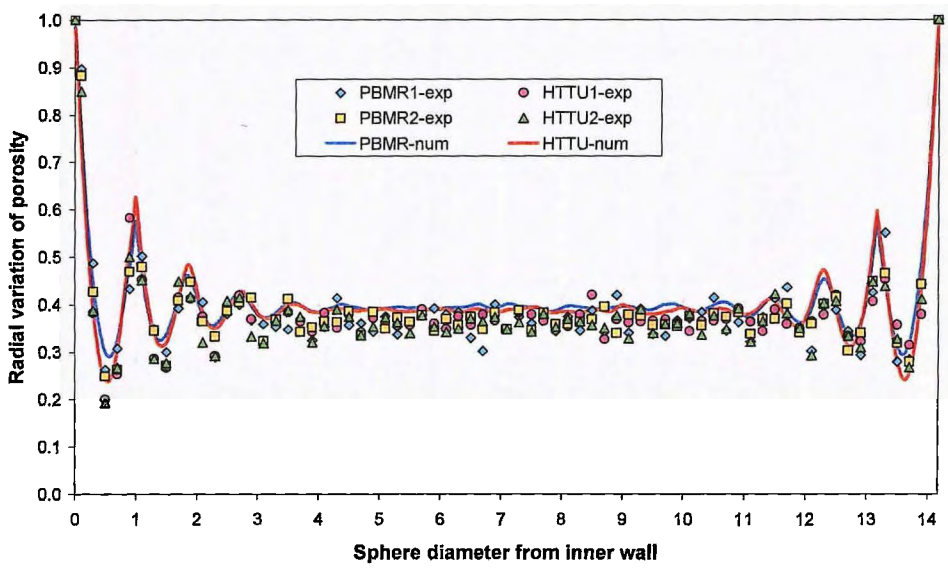

Figure 2.3: Experimental and numerical results for an annular packed bed (Du Toit, 2008:3076)

In an experimental study, Zou & Yu (1995:1505) investigated the thickness effect of a randomly packed bed of spheres in a cylindrical container with diameter D. The dependence of d_p/H and d_p/D on bulk porosity under loose and dense random packing conditions were investigated. Loose packing conditions refer to the case in which a bed is packed loosely and dense packing conditions refer to the case in which the bed is shaken for a certain period in order to achieve a denser packing. Figure 2.4 displays the results obtained by Zou & Yu (1995:1505).

Zou & Yu (1995:1505) emphasised that the influence of the thickness effect on porosity can be discarded if the value of d_p/H is sufficiently small. This explains why many investigators can obtain reasonably accurate porosity calculations without considering the thickness effect. Results demonstrated that the bulk porosity for both the loose and dense randomly packed beds start to increase in the vicinity of $d_p/H > 0.05$. A variation in bulk porosity between $0.395 < \varepsilon_b \leq 0.46$ was observed when $0.05 < d/H \leq 0.4$ in the dense randomly packed case. No correlations were proposed by Zou & Yu (1995:1505) in this regard.

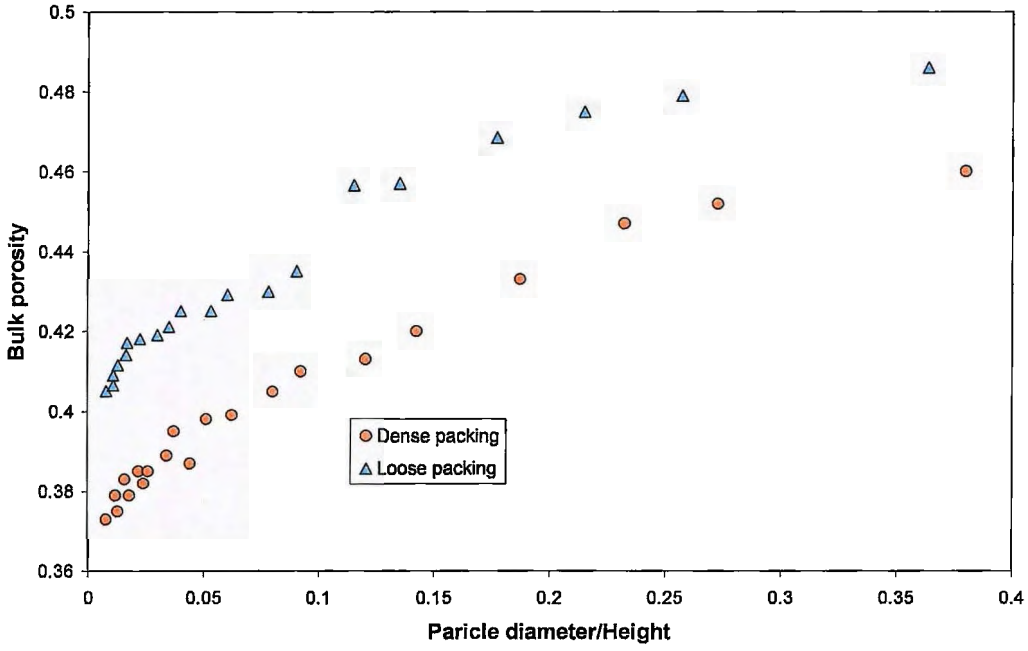

Figure 2.4: Experimental results displaying the thickness effect on bulk porosity for a given $d_p/D = 3/74$ ratio
(Zou & Yu, 1995:1505)

Correlations used to predict the variation in porosity can be classified into two categories: those that attempt to describe the oscillatory behaviour of the variation in the porosity and those that attempt to describe the variation of the averaged porosity using an exponential expression (Du Toit, 2008:3077). An overview is given in Table 2.1 summarising the correlations found in literature to describe the oscillatory behaviour of the variation in porosity. Several cylindrical bed correlations were rewritten to account for annular packed beds and others were left as presented in the original literature.

In the case of Mueller's (1999:2458) correlation there are various variations and empirical constants for which appropriate values are required. However, Theuerkauf *et al.* (2006:92) demonstrated that the Bessel function of the first kind J_0 does not provide an accurate representation of the void fraction in the near-wall region between $0 \leq z \leq 0.5$. For this reason the correlation developed by Mueller (1999:2458) is only summarised for the sake of completeness.

Table 2.1: Summary of the oscillatory porosity correlations in the radial direction

RESEARCHER/S	CORRELATION	PARAMETERS	EQ. NUM
Martin (1978:913)	$\varepsilon(x)=\begin{cases}\varepsilon_{min}+(1+\varepsilon_{min})x^2, & -1\le x<0\\ \varepsilon_b+(\varepsilon_{min}-\varepsilon_b)e^{-x/4}\cos\left(\frac{\pi}{C}x\right), & x\ge 0\end{cases}$	$x=2\frac{R-r}{d_p}-1$ $C=\begin{cases}0.816 & D/d_p=\infty\\ 0.876 & D/d_p=20.3\end{cases}$ $\varepsilon_{min}=0.20-0.26$	(2.3)
Cohen & Metzner (1981:359)	$\frac{1-\varepsilon(z)}{1-\varepsilon_b}=4.5\left[z-\frac{7}{9}z^2\right] \quad z\le 0.25$ $\frac{\varepsilon(z)-1}{1-\varepsilon_b}=a_1e^{(-a_2z)}\cos[a_3z-a_4]\pi \quad 0.25<z<8$ $\varepsilon(z)=\varepsilon_b \quad 8\le z\le\infty$	$z=\frac{R-r}{d_p}$ $a_1=0.3463,\ a_2=0.4273$ $a_3=2.4509,\ a_4=2.2011$	(2.4)
Ridgway & Tarbuck (1968:1147) Kamiuto *et al.* (1989:213)	*For* $0\le z\le 0.6$ $\varepsilon(z)=1-3.10036z+3.70243z^2-1.24612z^3$ *For* $0.6<z\le(R_0-R_i)/2d_p$ $\varepsilon(z)=-0.1865\exp\left(-0.22z_m^{1.5}\right)\cos(7.66z_m)+\varepsilon_b$	$z=\frac{r-R_i}{d_p},\quad R_i\le r\le\frac{R_0+R_i}{2}$ $z=\frac{R_0-r}{d_p},\quad \frac{R_0+R_i}{2}\le r\le R_0$ $z_m=z-0.6$	(2.5)
Mueller (1992:269)	$\varepsilon(r)=\varepsilon_b+(1-\varepsilon_b)J_0\left(a\frac{r}{d_p}\right)\times\exp\left(-b\frac{r}{d_p}\right)$	$a=\begin{cases}7.45-\frac{3.15}{D/d_p} & 2.02\le D/d_p\le 13.0\\ 7.45-\frac{11.25}{D/d_p} & 13.0\ge D/d_p\end{cases}$ $b=0.315-\frac{0.725}{D/d_p},\ \varepsilon_b=0.365+\frac{0.22}{D/d_p}$	(2.6)
De Klerk (2003:2022)	$\varepsilon(z)=2.14z^2-2.53z+1 \quad z\le 0.637$ $\varepsilon(z)=\varepsilon_b+0.29\exp(-0.6z)\times\left[\cos(2.3\pi(z-0.16))\right]+0.15\exp(-0.9z) \quad z>0.637$	$z=\frac{r-R_i}{d_p},\quad R_i\le r\le\frac{R_0+R_i}{2}$ $z=\frac{R_0-r}{d_p},\quad \frac{R_0+R_i}{2}\le r\le R_0$	(2.7)

The correlations presented in Table 2.1 were evaluated by comparing them with the numerical results of Du Toit (2008:3077) and the results are presented in Figure 2.5. The bulk porosity was taken as $\varepsilon_b = 0.385$, as with the results obtained in the numerical calculations. In the case of Martin's (1978:913) correlation, the minimum porosity was taken as $\varepsilon_{min} = 0.245$, in accordance with the numerical results and the constant in the equation was taken as $C = 0.876$. Du Toit (2008:3077) noted that in the case of Cohen & Metzner's (1981:359) correlation the dimensionless distance x from both walls in the middle of the annulus is less than eight and the correlation therefore never achieves the bulk value for the porosity.

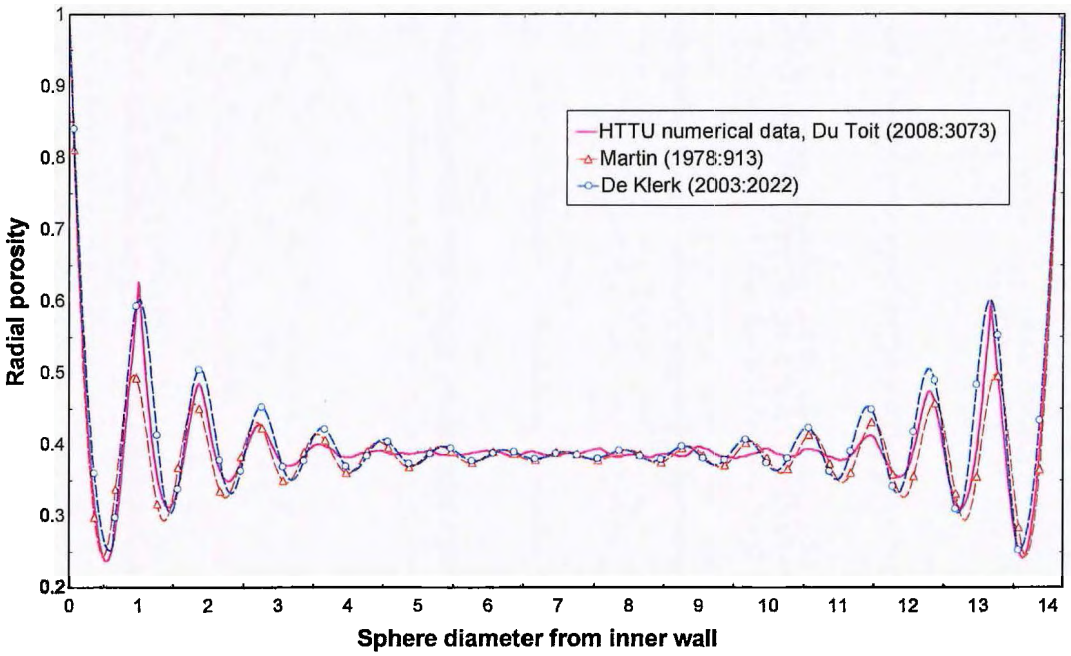

Figure 2.5: Comparison between radial oscillatory porosity correlations

Du Toit (2008:3077) found that Martin's (1978:913) correlation best fits the numerical results. However, after comparing the correlations displayed in Table 2.1 with the numerical results of Du Toit (2008:3077), it was found that De Klerk's (2003:2022) correlation gives a better prediction of the oscillatory variation in the radial porosity, particularly at $z = 1$ (Figure 2.5).

In some codes, such as the RANS CFD codes, the presence of spheres is modelled implicitly by assuming that the average porosity decays exponentially from the wall (Vortmeyer & Schuster, 1983:1691). Table 2.2 summarises all relevant correlations to determine the variation in porosity exponentially. In Table 2.1 and Table 2.2 it is important to note that R_i refers to the inner radius of the annulus and R_0 refers to the outer radius in an annular packed bed.

The parameter ε_0 in Eq. (2.8) is taken by Vortmeyer & Schuster (1983:1691), Cheng & Hsu (1986:1843), and Hunt & Tien (1990:2751) as equal to the bulk porosity $\varepsilon_0 = \varepsilon_b$, while Sodré & Parise (1998:265) take $\varepsilon_0 = \varepsilon_\infty$, where ε_∞ is defined as the porosity of an infinite bed. As Du Toit (2008:3073) explains, the value of C is taken to give a porosity of one at the wall interface. Therefore, Cheng & Hsu (1986:1843) assume $C = 1$, where the value of N is taken to be $N = 2$ by Vortmeyer & Schuster (1983:1691) and Cheng & Hsu (1986:1843), while Hunt & Tien (1990:2751) use a value of $N = 6$ for spheres. Furthermore, Sodré & Parise (1998:265) proposed that the value of N be obtained from Eq. (2.9), which must be solved iteratively with the average bed porosity for the annulus $\bar{\varepsilon}$.

Table 2.2: Summary of the exponential porosity correlations in the radial direction

RESEARCHER/S	CORRELATION	EQ. NUM
Vortmeyer & Schuster (1983:1691)	$\varepsilon(r)=\varepsilon_0\left[1+C\exp\left(-N\frac{r-R}{d_p}\right)\right], \quad R_i \le r \le \frac{R_0+R_i}{2}$ $\varepsilon(r)=\varepsilon_0\left[1+C\exp\left(-N\frac{R_0-r}{d_p}\right)\right], \quad \frac{R_0+R_i}{2} \le r \le R_0$	(2.8)
Sodré & Parise (1998:265)	**PARAMETER** $N=\frac{2C\varepsilon_\infty d_p\left[1-\exp\left(-N(R_0-R_i)/2d_p\right)\right]}{\left(\bar{\varepsilon}-\varepsilon_\infty\right)(R_0-R_i)}$ $\bar{\varepsilon}=0.3517+0.387\frac{d_p}{2(R_0-R_i)}$	(2.9)
White & Tien (1987:291)	**CORRELATION** $\varepsilon(r)=\left[1+\left(\frac{1-\varepsilon_b}{\varepsilon_b}\right)\sqrt{1-\exp\left(-2\frac{r-R_i}{d_p}\right)}\right]^{-1}$ for $R_i \le r \le \frac{R_0+R_i}{2}$ $\varepsilon(r)=\left[1+\left(\frac{1-\varepsilon_b}{\varepsilon_b}\right)\sqrt{1-\exp\left(-2\frac{R_0-r}{d_p}\right)}\right]^{-1}$ for $\frac{R_0+R_i}{2} \le r \le R_0$	(2.10)

The comparison between the exponential porosity correlations displayed in Table 2.2 and numerical results for the HTTU are displayed in Figure 2.6. Du Toit (2008:3077) noted that the correlation of Sodré & Parise (1998:265) failed to corroborate the results obtained by the other correlations and proposed that ε_∞ be substituted by ε_b in the bulk region of the annulus and $\bar{\varepsilon}$ be substituted with the average porosity for the annulus obtained from numerical results. After careful examination, Du Toit (2008:3077) found that the correlation of Hunt & Tien (1990:2751) gives the best representation of the averaged variation of porosity in the radial direction.

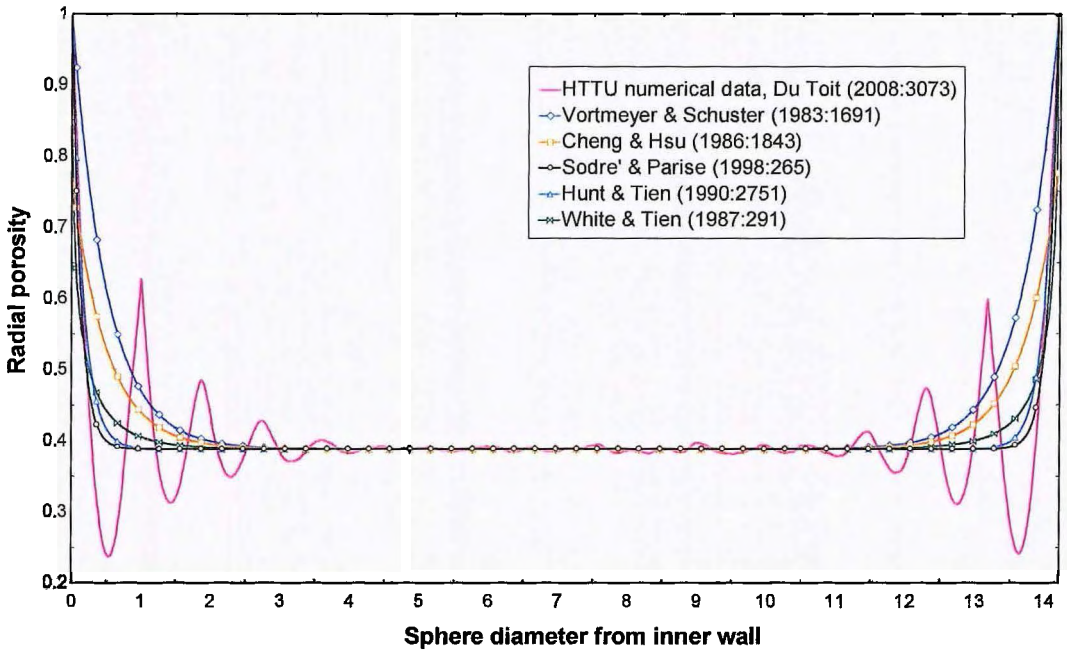

Figure 2.6: Comparison between radial exponential porosity correlations (Du Toit, 2008:3078)

2.2.2 COORDINATION NUMBER

The coordination number, also known as the kissing number, is the number of spheres in contact with the sphere under consideration. Determining the coordination number is very useful for modelling transport phenomena through packed beds as noted by Goodling & Khader (1985:53). They conducted experimental studies to determine the coordination number for 6.35 mm uniform-sized spheres, concluding that the average coordination number is approximately eight for a randomly packed bed with an average porosity of 0.39.

Various researchers, such as Rumpf (1958:144), Meissner *et al.* (1964:202), Ridgeway & Tarbuck (1967:384), have endeavoured to derive correlations that can predict the average coordination number for a given porosity in the bulk region of a randomly packed bed. Suzuki *et al.* (1981:482) present a summary of all these empirical correlations. A revised summary of these correlations is given in Table 2.3. There are significant differences when these correlations are plotted against one another as displayed in Figure 2.7. One aspect to be noted is that the empirical correlations shown in Table 2.3 are not valid in the near-wall region of a randomly packed bed, although several boundary conditions clearly state its validity up to a porosity of one. The main focus of the researchers was to quantify the bulk region of a packed bed and therefore the correlations presented in Table 2.3 are valid up to higher porosities in the bulk region for different types of packings.

Table 2.3: Equations for relation between average coordination number and porosity

RESEARCHER/S	CORRELATION	VALIDITY	EQ. NUM
Rumpf (1958:144)	$\overline{N}_C = 3.1/\varepsilon$	$(0.2595 \le \varepsilon \le 1)$	(2.11)
Meissner *et al.* (1964:202)	$\overline{N}_C = 2e^{2.4(1-\varepsilon)}$	$(0.2595 \le \varepsilon \le 1)$	(2.12)
Ridgeway & Tarbuck (1967:384)	$\varepsilon = 1.072 - 0.1193\overline{N}_C + 0.00431\overline{N}_C^2$	$(0.2595 \le \varepsilon \le 1)$	(2.13)
Haughey & Beveridge (1969:130)	$\overline{N}_C = 22.47 - 39.39\varepsilon$	$(\varepsilon \le 0.5)$	(2.14)
Nakagaki & Sunada (1968:651)	$\overline{N}_C = 1.61\varepsilon^{-1.48}$ $\overline{N}_C = 4.28\times10^{-3}\varepsilon^{-17.3} + 2$	$(\varepsilon \le 0.82)$ $(\varepsilon > 0.82)$	(2.15)
Smith *et al.* (1929:1271)	$\overline{N}_C = 26.49 - 10.73/(1-\varepsilon)$	$(\varepsilon \le 0.595)$	(2.16)
Gotoh (1978:220)	$\overline{N}_C = 20.7(1-\varepsilon) - 4.35$ $\overline{N}_C = 36(1-\varepsilon)/\pi$	$(0.3 \le \varepsilon \le 0.53)$ $(\varepsilon > 0.53)$	(2.17)
Suzuki *et al.* (1981:482)	$\overline{N}_C = 2.812\dfrac{(1-\varepsilon)^{-1/3}}{(b/d_p)^2\left[1+(b/d_p)^2\right]}$ where $(1-\varepsilon)^{-1/3} = \dfrac{1+\left(\frac{b}{d_p}\right)^2}{1+\left(\frac{b}{d_p}\right)e^{(d_p/b)^2}Erfc\left(\frac{d_p}{b}\right)}$	$(0.2595 \le \varepsilon \le 1)$	(2.18)
Yang *et al.* (2000:3900)	$\overline{N}_C = 2.02\dfrac{1+87.38(1-\varepsilon)^4}{1+25.81(1-\varepsilon)^4}$	$(0.39 \le \varepsilon \le 1)$	(2.19)
Zhang *et al.* (2001:23)	$\overline{N}_C = \dfrac{1}{0.183 - 659.248(1-\varepsilon)^{20.961}}$	$(0.37 \le \varepsilon \le 0.45)$	(2.20)

In this study, the same numerically generated annular packed bed data set used by Du Toit (2008:3073) for porosity calculations was used in an attempt to determine the average coordination number in the radial direction. Liu *et al.* (1999:443) demonstrated that the average coordination number is independent of sample size in a numerical simulation when the number of spheres analysed is above 5000. Therefore, for the sake of completeness ± 20000 spheres were used. Spheres whose centre coordinates were between five pebble diameters from the bottom to a height of 1.2 m was used to calculate average coordination numbers. This is chosen as such to eliminate any disruption in the packing structure due to the bottom support influencing the packing structure and also to a height right up to the top of the bed since there no disruption is present (thickness effect eliminated). In addition, the coordination numbers of spheres whose centres are within one pebble diameter from the above-mentioned upper and lower limits were not used to obtain the average coordination numbers.

The coordination number of the sphere under consideration was obtained by calculating the distance between the considered sphere centre 1 and adjacent sphere centres j (Appendix G.1). It was then assumed that the two spheres are in contact when $d \leq d_p + 0.002\,mm$. The distance between two spheres was calculated by:

$$d = \sqrt{(x_1 - x_j)^2 + (y_1 - y_j)^2 + (z_1 - z_j)^2} \tag{2.21}$$

where x, y and z are the coordinates of the centre of a specific sphere.

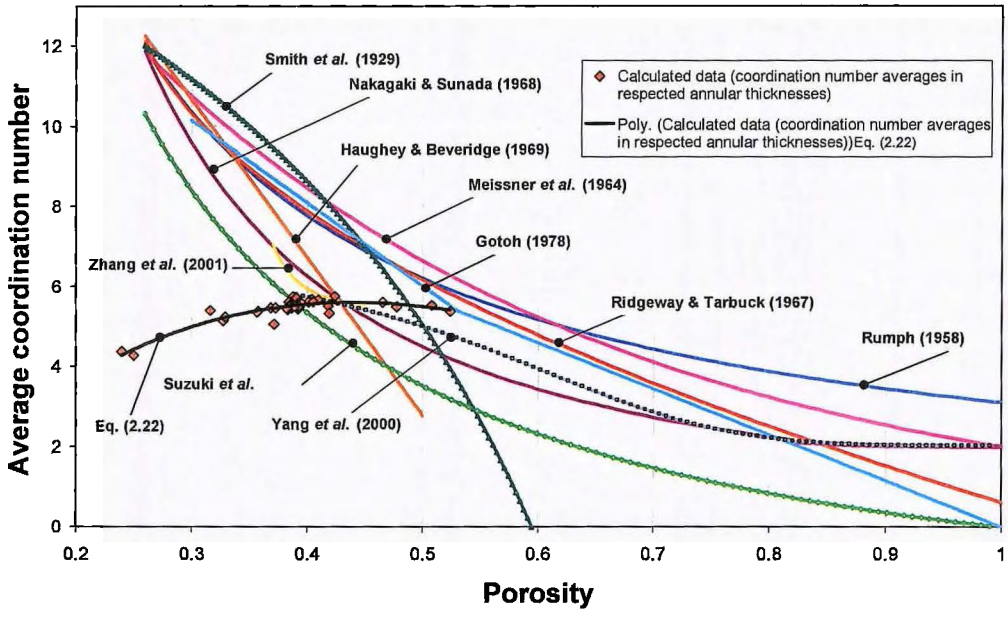

Figure 2.7: Comparison between various coordination number models (see Table 2.3)

The radial distribution of the average coordination number was obtained by calculating the average coordination number of the spheres whose centres fell inside a specific annular thickness (radial slices). Annular radial thicknesses of $1/4\,d_p$, starting at $1/2\,d_p$, from any wall were used. This was done according to the method described by Goodling & Khader (1985:53). Results for the full radial distribution of the HTTU annular bed are displayed in Figure 2.8, where the average coordination number in the bulk region is found to be approximately 5.62. This value is in line with the value of 6.13 that was presented by Lochmann *et al.* (2006:1397), who used a numerical packing algorithm to determine the coordination number for a randomly packed bed in the bulk region with a porosity of $\varepsilon = 0.36$. In addition, Bernal & Mason (1960:910) found the coordination number in another numerically generated packed bed geometry to be approximately 5.5 with a porosity in the region of $\varepsilon = 0.40$.

Nonetheless, the numerical results compare well with the experimental trends presented by Goodling & Khader (1985:53), who determined the coordination number experimentally for

much smaller spheres. They also observed a reduction of average coordination number at around two pebble diameters from the wall.

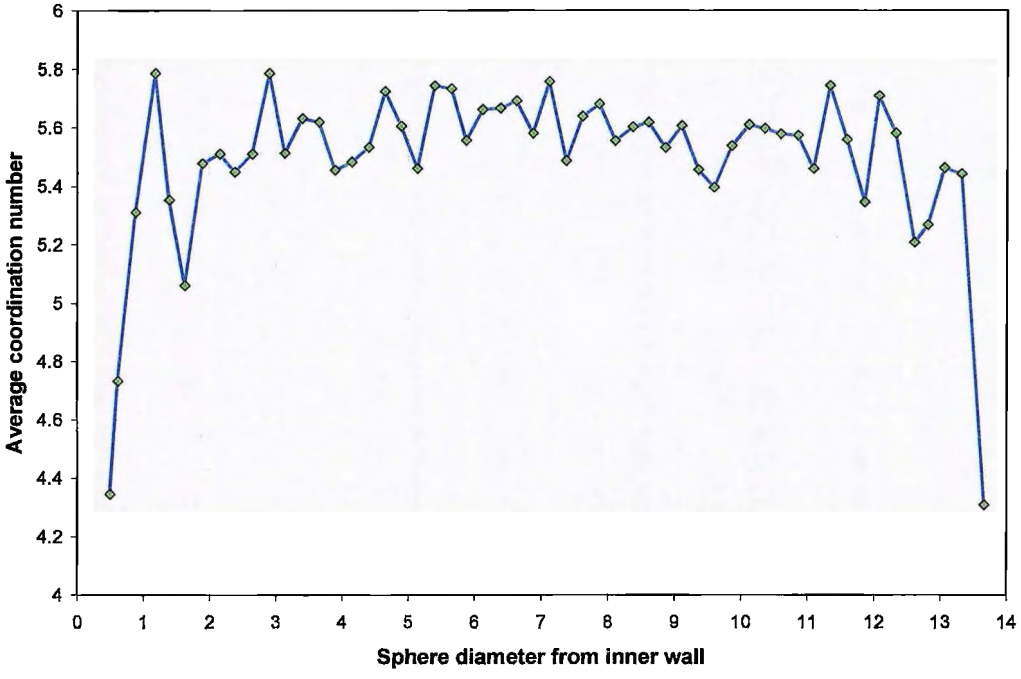

Figure 2.8: Average coordination number of the High Temperature Test Unit

Furthermore, a relationship between porosity and average coordination number was obtained by plotting the calculated data (coordination number averages in respected annular thicknesses) against the porosity results of Du Toit (2008:3077) at the same radial position (Figure 2.7). From Figure 2.7, it is evident that the correlation proposed by Suzuki *et al.* (1981) is the only correlation that accurately predicts the average coordination number in the bulk region of the HTTU.

However, none of the existing models accurately predicts the relationship between average coordination number and porosity at near-wall conditions, where on average the bulk porosity varies between $0.38 > \varepsilon > 0.42$. This emphasises the above-mentioned statement that the correlations presented in Table 2.3 are not valid in the near-wall region and the focus of the researchers was mainly on the bulk region for different types of packings.

A new correlation (Eq. 2.22) was therefore derived in this study to predict the average coordination number with respect to the radial porosity variation in an annular randomly packed bed. This was done using a third order polynomial curve fit through the calculated data presented in Figure 2.7.

It was decided to derive average coordination number as a function of porosity, as porosity is the most widely used parameter to quantify a packing structure. However, it must be noted that average coordination number can also be written as a function of sphere diameters from

inner wall. This derived correlation now implicitly includes the near-wall region via the higher and lower average porosity values and is as follows:

$$\bar{N}_c = 25.952\varepsilon^3 - 62.364\varepsilon^2 + 39.724\varepsilon - 2.0233 \qquad (0.2398 \le \varepsilon \le 0.54) \qquad (2.22)$$

2.2.3 CONTACT ANGLES

The contact angle is defined as the angle between the line connecting the centre points of two spheres in contact and the line perpendicular to the direction of the heat flux, as illustrated in Figure 2.9.

Sui & Lee (2000:3922) recognised the importance of the contact angle when simulating the effective thermal conductivity in ordered packings. They derived a correlation predicting the thermal resistance between two adjacent spheres given a certain contact angle. In this study a new contact angle definition and correlation are developed for randomly packed beds. A contact angle of $\phi_c = 0°$ implies that the conduction form the adjacent sphere j contributes nothing to the overall heat transfer between spheres j and 1, while a contact angle of $\phi_c = 90°$ implies maximum contribution to heat transfer between the two spheres.

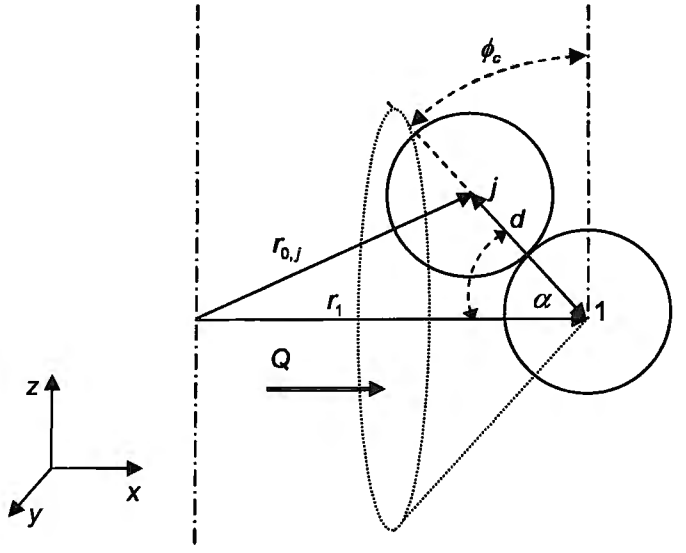

Figure 2.9: Contact angle between two spheres

Therefore, a procedure was developed to calculate the average contact angles when the centre coordinates and diameters of all the spheres are known. The radii r_1 and $r_{0,j}$ are calculated as follows:

$$r_1 = \sqrt{x_1^2 + y_1^2} \qquad (2.23)$$

and

$$r_{0,j} = \sqrt{x_j^2 + y_j^2 + (z_1 - z_j)^2} \tag{2.24}$$

Using the law of cosine, the following relation is used to calculate the contact angle between two spheres:

$$r_{0,j}^2 = r_1^2 + d^2 - 2r_1 d\cos(\alpha) \tag{2.25}$$

We have that $\alpha + \phi_c = 90°$, therefore, substituting into Eq. (2.25) and rearranging yields the following:

$$\phi_c = \sin^{-1}\left(\frac{r_{0,j}^2 - r_1^2 - d^2}{-2r_1 d}\right) \tag{2.26}$$

where d is the distance between sphere 1 and j calculated with Eq. (2.21). This distance is usually close to d_p. However, this distance could be slightly less owing to the deformation of the spheres as a result of the external forces acting on the two spheres. The radial distribution of the contact angle is obtained for annular thicknesses (radial slices) of $1/4\,d_p$ using the same method employed to determine the average coordination number. It must be emphasised that only positive values of ϕ_c contribute to overall heat transfer between adjacent spheres. For this reason, average contact angles in the specific annular thickness are calculated from the annulus to the outer reflector $(+\phi_c)$, as well as from the outer reflector to the annulus $(-\phi_c)$, as displayed in Figure 2.10. From Figure 2.10 it can be seen that the contact angle differs when calculated moving towards a wall and when calculated moving away from a wall.

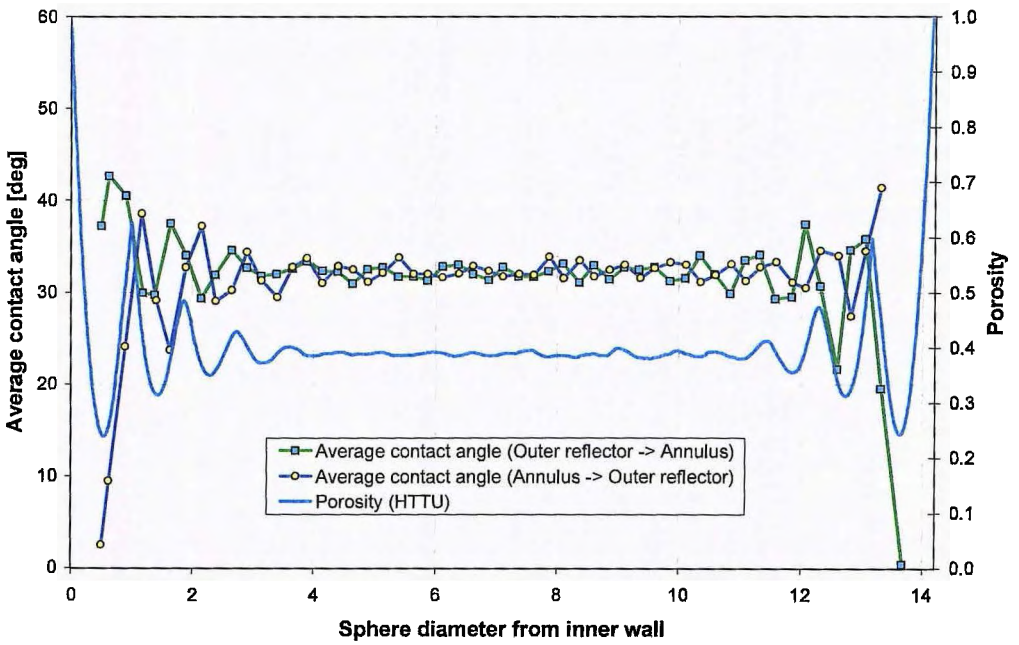

Figure 2.10: Average contact angles calculated in two radial directions for the High Temperature Test Unit

An average total contact angle is further calculated, taking the absolute values of all the contact angles for a considered sphere and calculating the average contact angle in the annular thicknesses. This eliminates the problem of a positive or negative contact angle with respect to the direction of heat flux, as displayed in Figure 2.11, where $+\phi_{c,1-2}$ and $\left|-\phi_{c,1-3}\right|$ is considered in calculating the average total contact angle ϕ_c.

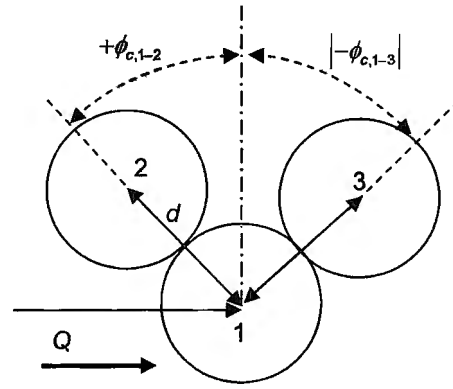

Figure 2.11: Calculation of average total contact angles

In Figure 2.12 it is also shown that the average total contact angle at the inner reflector, which has a convex surface, does not differ much in magnitude from that at the outer reflector, which has a concave surface. However, it would appear that the effect of the annulus (inner wall) penetrates slightly deeper into the radial direction of the bed compared to that of the outer wall.

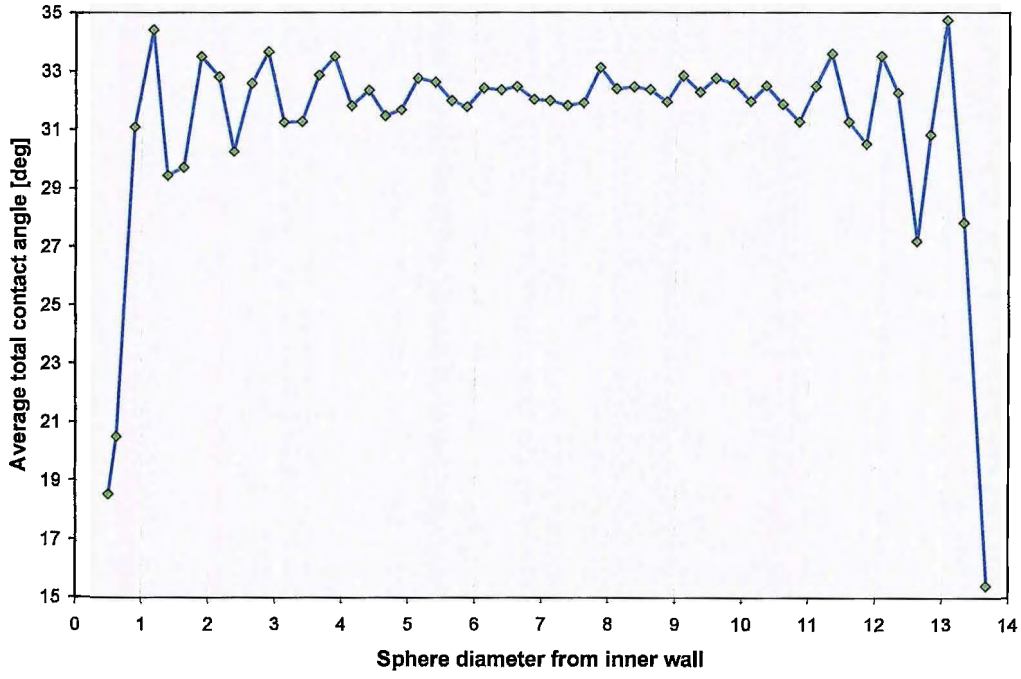

Figure 2.12: Average total contact angle calculated in the radial direction for the High Temperature Test Unit

It is interesting, and expected, that the average total contact angle decreases when approaching a wall. For this reason, a relationship between average coordination number and average total contact angle was obtained by plotting the two quantities against one another. Each data point value was compared at the same radial position. Results are depicted in Figure 2.13. Fitting a second order polynomial curve through the results yields the following correlation:

$$\bar{\phi}_c = -6.1248\bar{N}_c^2 + 73.419\bar{N}_c - 186.68 \qquad (2.27)$$

The average contact angle in the bulk region of the HTTU was found to be $\bar{\phi}_c = 32.28°$. It must also be noted that like average coordination number, contact angle can also be written as a function of sphere diameters from inner wall.

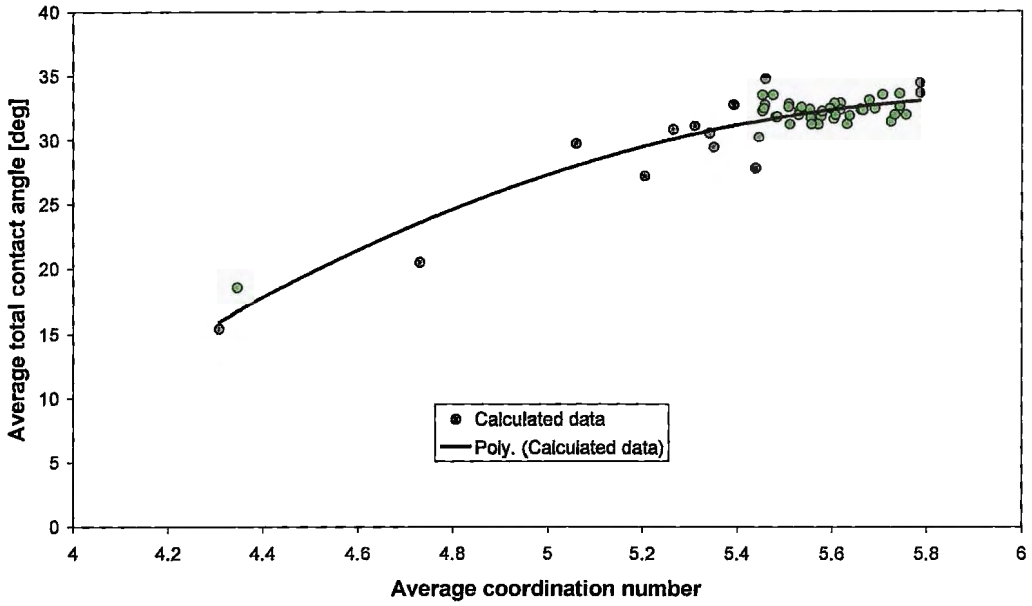

Figure 2.13: Average total contact angle versus average coordination number for data points at the same radial position in the High Temperature Test Unit

One must note that the aforementioned analysis was done comparing the average coordination number with the average total contact angle in the same annular thickness. A further investigation is done comparing the average total contact angle with the radial porosity calculated by Du Toit (2008:3077), to see if a smoother function between these two variables exists. It is evident from the results in Figure 2.14 that a relation between average total contact angle and radial porosity does exist. However, it would appear that there are more scattering around the curve fit than in Figure 2.13.

Furthermore, if the radial slice thickness is reduced from $15mm$ to $1.5mm$ ($0.25d_p$ to $0.025d_p$), Figure 2.14 changes to Figure 2.15, which further demonstrates that the contact angle is not a smooth function of porosity. Therefore, Figure 2.15 clearly illustrates the

limitations of simplifying the porous structure and must be treated accordingly.

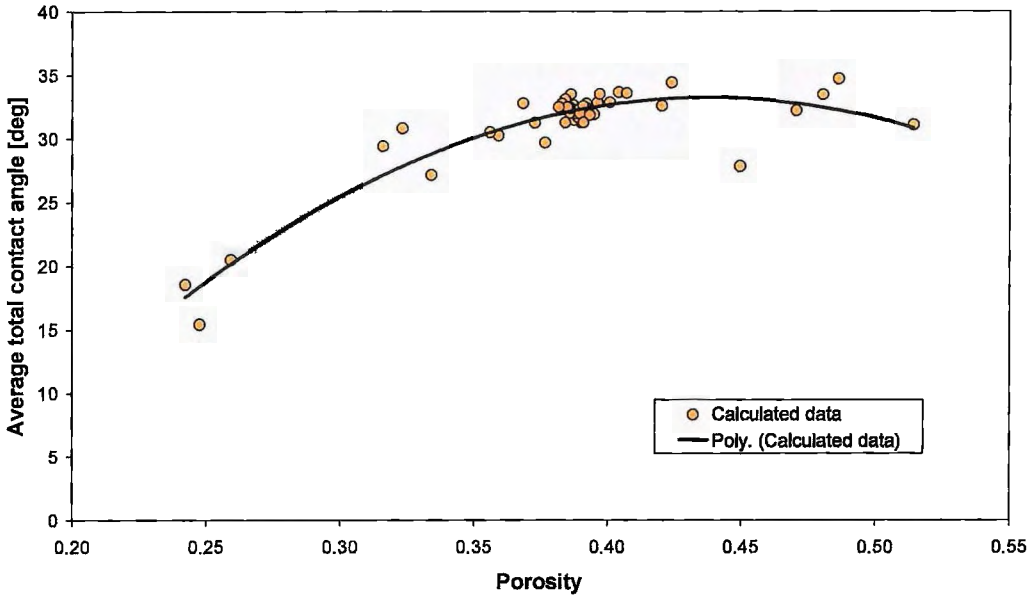

Figure 2.14: Average total contact angle versus porosity for data points at the same radial position in the High Temperature Test Unit

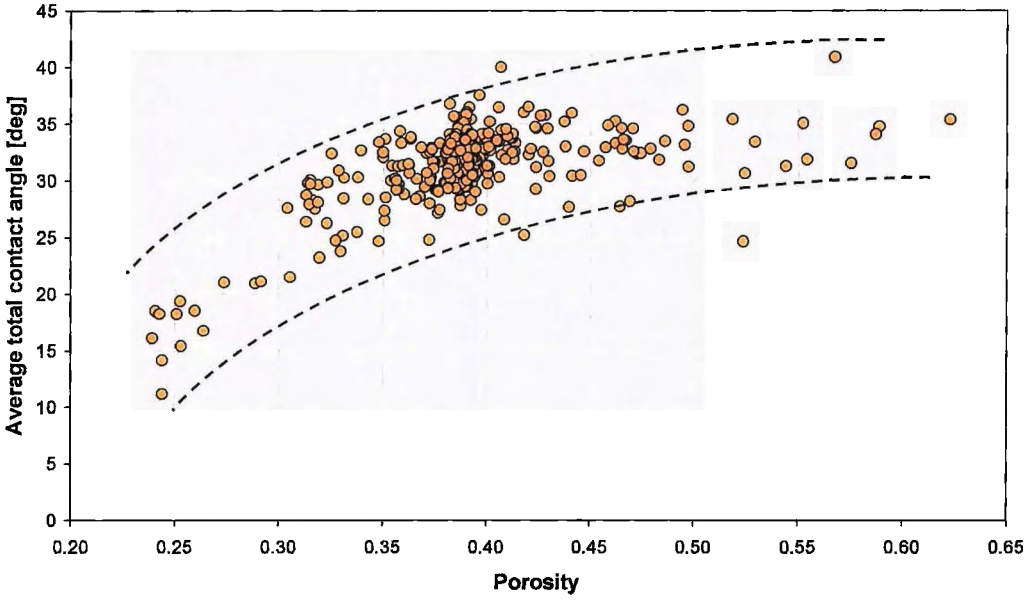

Figure 2.15: Calculated average total contact angle versus porosity with 1.5 mm radial slice thicknesses in all packing regions

2.2.4 RADIAL DISTRIBUTION FUNCTION

The Radial Distribution Function (RDF) is defined as the probability of finding one pebble centre at a given distance r from a certain reference position. The RDF is of particular importance in this study to better quantify the discretization length in the near-wall region when calculating effective thermal conductivity. The RDF is defined in a three-dimensional system as:

$$g_{3D}(r) = \frac{n(r)}{4\pi r^2 \Delta r} \tag{2.28}$$

where $n(r)$ is the number of sphere centres situated in a radial slice at a distance between r and $r + \Delta r$ from the centre of a given pebble (Liu *et al.*, 1999:443). Tanemura (1986:157) suggested that the RDF also be quantified for a two-dimensional system by the following:

$$g_{2D}(r) = \frac{n(r)}{2\pi r \Delta r} \tag{2.29}$$

The RDF for the HTTU experiment with $\Delta r = 1.5mm$ can now be obtained based on the two-dimensional formulation and is displayed in Figure 2.16. Superimposed onto Figure 2.16 is the numerical porosity distribution obtained by Du Toit (2008:3077). It is evident from Figure 2.16 that the porosity distributions at the inner and outer reflector walls are very similar. However, there are some differences in the two-dimensional RDF between the two reflector walls. That said, in this study it is assumed that the packing structure at the inner and outer reflector walls is similar based on radial porosity observations.

From Figure 2.16 one can see that the higher RDF peaks in the near-wall regions coincides with the lower peaks of the radial porosity distribution. This is intuitively true as a high probability of finding sphere centres at a given distance from a reflector wall must result in a lower porosity. It can be seen that the peaks of the RDF are not perfectly aligned with the lowest values of porosity. This could perhaps be attributed to the fact that the number of spheres used in the calculation of the porosity and RDF is not exactly the same.

Furthermore, another aspect to consider in the near-wall region is the length scales or discretisation lengths of the porous structure. Porous structure parameters such as porosity, coordination number and contact angle can be obtained employing a fine discretisation of the empirical porosity equations displayed previously. However, in reality only one contact angle and one coordination number value can exist between two adjacent spheres and a fine discretisation may be misleading. This has lead to a further simplification of the description of the porous structure in the near-wall region denoted as a porosity correction factor ε^*, valid for $0.5 < z \leq 3.8$.

The porosity correction factor ε^* is developed as an empirical correlation through porosity points where the probability of finding sphere centres in the near-wall region is the highest as displayed in Figure 2.16. This is done to be used in collaboration with Eq. (2.22) to simulate a smoother reduction in average coordination number and contact angle in the near-wall region, implying the calculation of the porous structure parameters at the highest probabilities of finding sphere centres in the radial direction. This porosity correction factor is given by:

$$\varepsilon^* = -0.0127z^2 + 0.0967z - 0.2011 \tag{2.30}$$

for

$$z = \frac{r - R_i}{d_p}, \quad R_i \le r \le \frac{R_0 + R_i}{2} \tag{2.31}$$

or

$$z = \frac{R_0 - r}{d_p}, \quad \frac{R_0 + R_i}{2} \le r \le R_0 \tag{2.32}$$

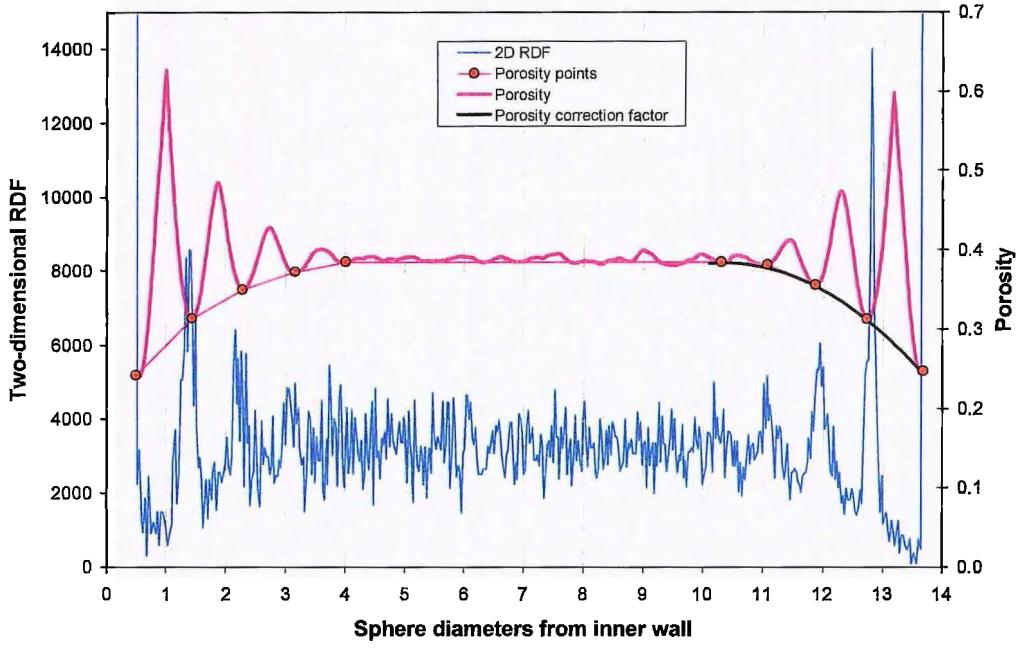

Figure 2.16: Two-dimensional radial distribution function for the High Temperature Test Unit ($\Delta r = 1.5mm$)

2.2.5 COORDINATION FLUX NUMBER

An important aspect that is not widely recognised in heat transfer calculations, is the actual number of spheres in contact with the sphere under consideration that contribute to heat transfer in a certain direction. This is of relevance in this study because it is one of the critical components in the derivation of the new Multi-sphere Unit Cell Model.

This parameter n is hereafter referred to as the coordination flux number. Kunii & Smith

(1960:71) endeavoured to define this value in a randomly packed bed and argued that for a basic loose packing the value of n should be $n = 1.5$ and for a more dense close packing the value n should be $n = 4\sqrt{3}$ for a porosity range of $0.26 \leq \varepsilon \leq 0.476$.

Coordination flux numbers were obtained in this study by calculating the contact angles described in Section 2.2.3 and counting the number of positive and negative contact angles respectively for the sphere under consideration. The average coordination flux number was then calculated in the inward and outward radial directions again taking annular radial thicknesses of $1/4d_p$, starting at $1/2d_p$, from any wall. The results of the average coordination flux number are presented in Figure 2.17. It was found that by approximating the coordination number as $n = \bar{N}_c/2$ gives adequate values for n, as displayed in Figure 2.17.

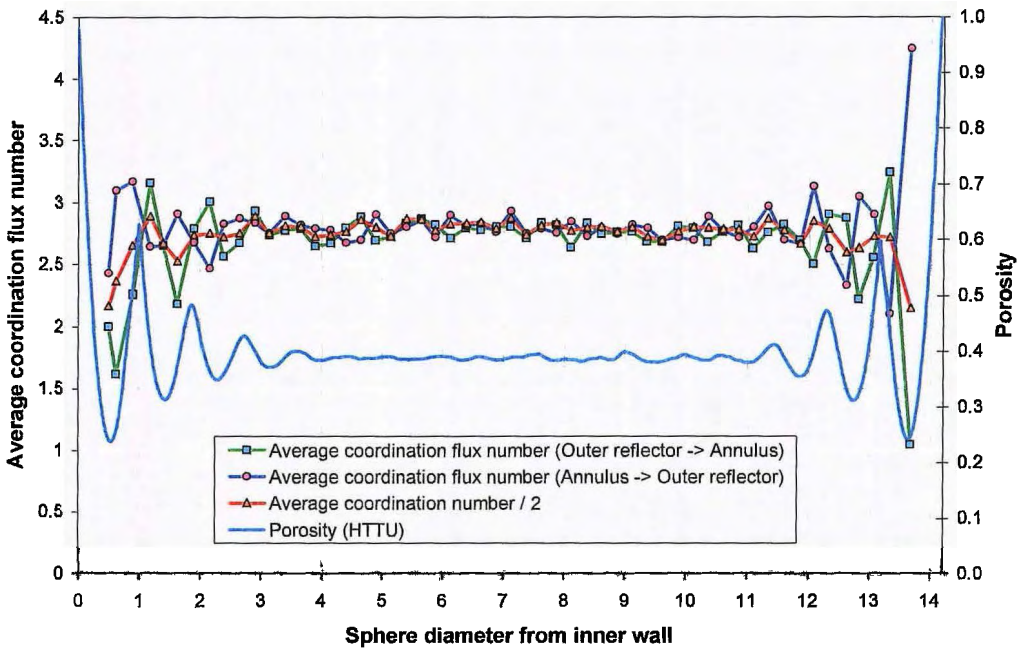

Figure 2.17: Average coordination flux number calculated in two radial directions in the High Temperature Test Unit

2.2.6 VORONOI POLYHEDRA

The Voronoi polyhedron is a concept that indicates the distinctive features of pebble arrangements in a space by means of space discretisation, and refers to the shape obtained by joining each element centre point to its nearest centre point (Cheng *et al.*, 1999:4199). The Voronoi polyhedron is of no particular relevance to this study, but is briefly mentioned for the sake of completeness in this literature investigation.

The Voronoi polyhedron is constructed in the following manner; consider line OP in Figure 2.18 (a). A boundary plane of a polyhedron is created by taking a perpendicular bisector of

line OP. This procedure is extended, resulting in a three-dimensional Voronoi polyhedron as displayed in Figure 2.18 (b).

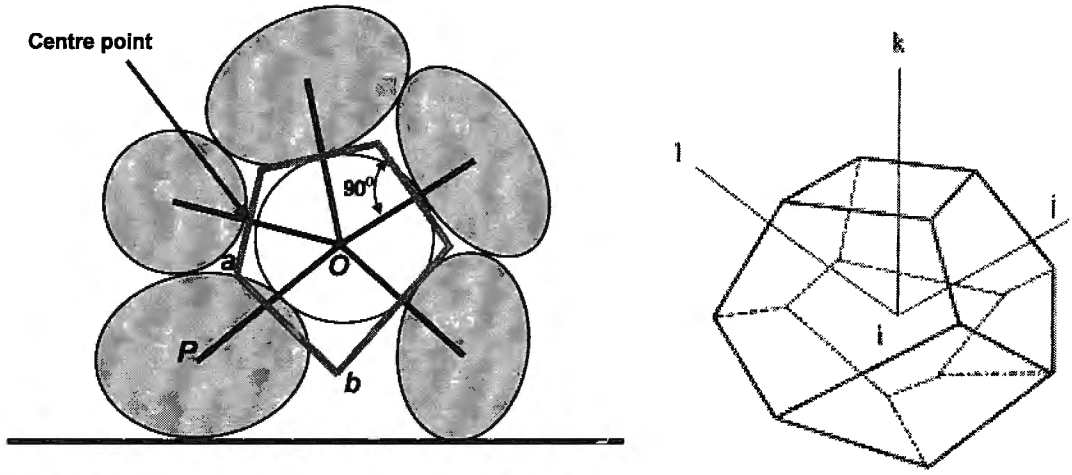

(a) Two-dimensional (Hinrichsen & Wolf, 2006:55)

(b) Three-dimensional (Cheng *et al.*, 1999:4199)

Figure 2.18: Schematic of a Voronoi polyhedron

A randomly packed bed can be discretised into an array of Voronoi polyhedra of various shapes and sizes. Cheng *et al.* (1999:4199) used these Voronoi polyhedra to simulate structure based heat transfer through a randomly packed bed. A graphical illustration of the Voronoi polyhera for a binary packing of 1000 spheres is presented in Figure 2.19.

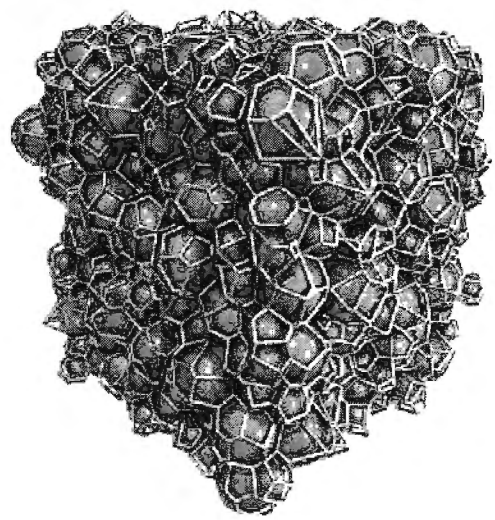

Figure 2.19: Schematic of Voronoi polyhedra for a binary packing of 1000 spheres (Lochmann *et al.*, 2006:1397)

2.3 STRUCTURED (ORDERED) PACKINGS

In the open literature such as presented in Kaviany (1991:127) ordered packing structures are classified into three different arrangements. These are Simple Cubic packing (SC), Body-centered Cubic packing (BCC) and Face-centred Cubic packing (FCC). Various researchers such as Suzuki *et al.* (1981:482) noted that the densest packing arrangement is FCC packing. Table 2.4, Figure 2.20 and Figure 2.21 present some important specifications on the various structural arrangements.

Siu & Lee (2000:3917) and Kaviany (1991:127) used these structured packing arrangements to quantify the porous structure in a randomly packed bed for calculating effective thermal conductivity. They argued that if the porosity ε in a randomly packed bed is within a certain porosity range, the porous structure will be analogous to that of a specific ordered packing structure.

Table 2.4: The comparison of coordination number and porosity with different arrangements

TYPE OF PACKING ARRANGEMENT	POROSITY	COORDINATION NUMBER	COORDINATION FLUX NUMBER
SC array	$\delta = 0.524, \left(\frac{\pi}{6}\right)$ $\varepsilon = 0.476$	6	1
BCC array	$\delta = 0.680, \left(\frac{\sqrt{3}\pi}{8}\right)$ $\varepsilon = 0.32$	8	4
FCC array	$\delta = 0.7405, \left(\frac{\pi}{3\sqrt{2}}\right)$ $\varepsilon = 0.2595$	12	4

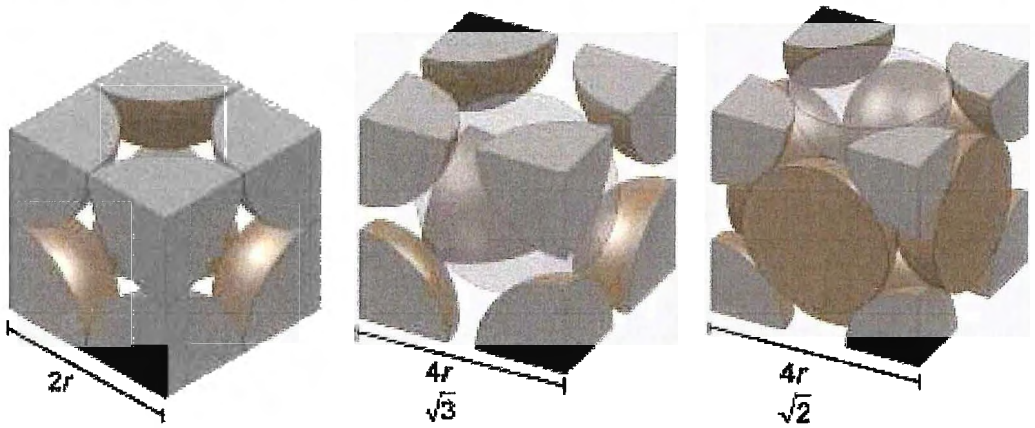

(a) SC (b) BCC (c) FCC

Figure 2.20: Ordered packing structures (Kaviany, 1991:129)

(a) SC (b) BCC (c) FCC

Figure 2.21: Ordered packing structures (Kaviany, 1991:129)

2.4 LIMITATIONS ON DEFINING PACKING STRUCTURE WITH POROSITY ONLY

In most existing effective thermal conductivity models, the porous structure is commonly quantified using porosity alone. Employing only porosity to quantify the porous structure in the effective thermal conductivity calculations is usually valid on condition that the model is used within specified porosity bounds. The most common simplification associated with these models is to assume some form of ordered packing, such as SC, BCC and FCC, in order to quantify the porous structure in the bulk and near-wall regions of a randomly packed bed.

When considering an ordered packing within the bulk region of a randomly packed bed, it may be presumed that either the porous structure may be close to SC or BCC with the porosity approaching quantities displayed in Table 2.4. However, the coordination number of those ordered packings is $N_c = 6$ for SC and $N_c = 8$ for BCC, while in the randomly packed bed used as the basis for this study it was found to be $\bar{N}_c = 5.62$. This comparison clearly demonstrates that the SC-ordered packing would be the best option to use. However, if one considers the coordination flux number, the magnitude for the SC-ordered packing is $n = 1$, while for a randomly packed bed in the bulk region it was actually found to be $n = \bar{N}_c/2 = 2.81$. This indicates clearly a significant difference when used in heat transfer calculations.

When comparing the near-wall region in a randomly packed bed to a FCC-ordered packing with a porosity of $\varepsilon = 0.2595$, important differences are also found. In the numerical porosity calculations for a randomly packed bed presented by Du Toit (2008:3077), it was shown that the porosity at $0.5d_p$ away from the wall is $\varepsilon = 0.2398$, which is very close to that of the FCC-ordered packing. However, there is a significant difference between the calculated coordination number in a randomly packed bed of $\bar{N}_c = \pm 4.35$ and that of the FCC-ordered

packing at $N_c = 12$. Therefore, defining porous structure using porosity alone is not sufficient.

2.5 CONCLUSION

The structure of a randomly packed annular pebble bed can be quantified with various methods and tools. It was found that in previous work the most widely used parameter to quantify the porous structure is porosity. Experimental and numerical procedures were developed and used by Du Toit (2008:3073) to compare porosity variation in the radial and axial directions of a randomly annular packed bed. It was further found that RDF, coordination number and Voronoi polyhedrons could also quantify the porous structure to some extent. Several parameters were developed in this chapter for a randomly packed bed to help quantify the porous structure in such a way to be used for effective thermal conductivity calculations. The limitations on using porosity as the main parameter to quantify porous structure were also indicated. A summary of relevant literature and derived parameters is illustrated in Figure 2.22.

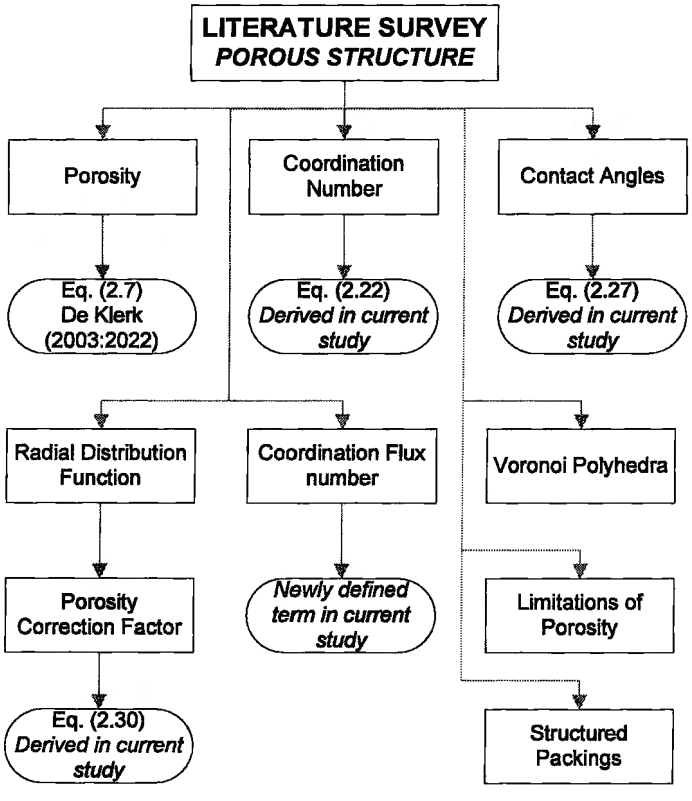

Figure 2.22: Literature survey porous structure flowchart